Magnetic Properties of Transition-Metal-Doped Tubular Gold Clusters: M@Au_{24} (M = V, Cr, Mn, Fe, Co, and Ni)

Aping Yang, Wei Fa, and Jinming Dong*

Group of Computational Condensed Matter Physics, National Laboratory of Solid State Microstructures, and Department of Physics, Nanjing University, Nanjing 210093, China

Received: September 3, 2009; Revised Manuscript Received: December 23, 2009

The energetic and magnetic properties of the tubular cluster Au_{24}, doped endohedrally by a 3d transition-metal atom M (M = V, Cr, Mn, Fe, Co, and Ni) have been investigated by the scalar relativistic density functional simulations. It is found that (1) these 3d transition-metal atoms can be encapsulated stably into the tubular Au_{24} and do not significantly perturb the atomic and electronic structures of the parent tubular Au_{24}, (2) the infrared (IR) spectra of the tubular Au_{24} cluster are significantly changed by the dopant atoms, inducing a characteristic absorption peak in the IR spectra of all the M@Au_{24}, and (3) protected by the tubular Au_{24}, the 3d states of the dopant atoms are largely localized, and the atom-like magnetism is retained for all the doped gold clusters, exhibiting 3, 6, 5, 4, 3, and 2 μ_B for V−Ni, respectively.

I. Introduction

Gold clusters Au_n have been subjected to extraordinary research, which is driven by their novel properties and various potential applications, such as catalysts, cell- and virus-active particles, and nanoscale electric and optical devices.[1−3] Because of the strong relativistic effects,[4] gold clusters exhibit intriguing geometrical structures and size-dependent evolution. For example, they favor the two-dimensional planar structures up to about $n = 12$,[4] cages at $n = 16-18$,[5] a perfect tetrahedron at Au_{20},[6] tubular structures at Au_{24} and Au_{26},[7,8] and fullerene-like cages of Au_{32}.[9]

Recently, however, increasing attention has been paid to gold-based bimetallic clusters[10−19] since an additional degree of freedom in the stoichiometry can offer a chemical versatility for finely tuning the gold clusters' properties and enhancing their potential applications.

Pyykkö and Runeberg[10] theoretically predicted a particularly stable icosahedral cluster W@Au_{12}, which was subsequently confirmed experimentally.[11] However, since the Au_{12} cage itself is unstable, the enhanced stability of the metal-doped Au_{12} cluster was attributed to relativistic effects, the 18-electron rule, and aurophilic attractions. Using combined photoelectron spectroscopy (PES) and density functional theory (DFT) calculations, Li et al.[17] investigated the electronic structure and magnetic properties in a series of transition-metal-doped Au clusters, MAu_6^- (M = Ti, V, Cr). It was found that the magnetic moments of the impurity transition-metal atoms are not quenched by the nonmagnetic gold host in the MAu_6 clusters, which are determined by the number of d electrons, localized in the atom-like unhybridized 3d orbitals of the dopants. Also, the discovery of empty Au_n cages at $n = 16-18$[5] stimulates increasing interest in a new class of endohedral doped gold cage clusters since a cage could hold a suitable impurity, tailoring the host gold cluster's properties in a desirable fashion.[20−27] For example, the endohedral structures of Cu@Au_{16}^- and Cu@Au_{17}^- have been validated by joint PES and DFT calculations,[20] in which the copper atom does not significantly perturb the electronic and atomic structures of the Au_{16}^- cage but simply donates its valence electrons to the surrounding gold cage. The Au_{16}^- cage, doped by different transition-metal atoms M (M = Fe, Co, and Ni), has also been investigated,[24] showing that all three kinds of magnetic atoms can be put inside of the Au_{16}^- cage but leading to a significant distortion of the parent cage structure. At the same time, their 4s electrons are found to transfer into the golden cage, and their 3d states remain largely localized, maintaining the atom-like magnetism in the doped clusters. Such a study shows that the Au_{16}^- cage can serve as a flexible host to protect the spins of the dopant magnetic atom.

On the other hand, inspired by synthesizing the multiwalled and single-walled gold nanotubes (SWGNTs),[25] the researchers predicted theoretically the possibility to form a hollow tubular Au_n cluster by closing a segment of the SWGNT, which is now considered to be a powerful candidate, competing in energy with other possible structures, such as the amorphous, the bulk fragment, and the cage-like ones. Fa et al.[7] first predicted the existence of tubular Au_{24} and Au_{26} by the guided simulation annealing plus DFT calculations. Successively, Xing et al.[26] and X. C. Zeng's group[27] verified the appearance of a tubular structure at $n = 24$ with different experimental techniques. It is obvious that the tubular Au_{24} structure can also accommodate a guest atom to form a new kind of endohedral tubular gold clusters. Therefore, it is very interesting to study in this paper the structural and magnetic properties of the tubular Au_{24} doped with different 3d transition-metal atoms M (M = V, Cr, Mn, Fe, Co, and Ni) by the scalar relativistic DFT calculations. It is found that all of the M@Au_{24} clusters still possess a tubular structure, in which the dopant atom is located in the center of the tubular Au_{24} cluster, carrying a large magnetic moment of 3, 6, 5, 4, 3, and 2 μ_B, respectively, for M = V, Cr, Mn, Fe, Co, and Ni. The following section introduces the DFT procedures adopted in our calculations. The obtained results and discussions are given in section III. Finally, the concluding remarks are offered in section IV.

II. Computational Details

Our numerical simulations were carried out with spin-polarized DFT at the level of a generalized gradient approxima-

* To whom correspondence should be addressed. E-mail: jdong@nju.edu.cn.

10.1021/jp908511m
Published on Web 03/01/2010

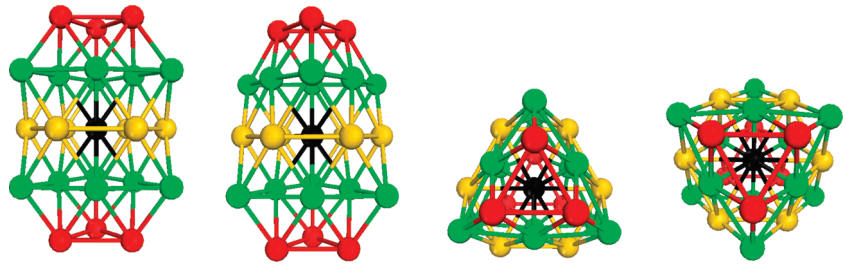

Figure 1. Optimized ground state (a) and the first-lying isomer (b) of the tubular M@Au_{24} clusters. (c, d) Their top views, respectively. Here, the center black ball represents the transition-metal dopant. For clarity, the capped atoms of the tubular structures are shown with red balls, while the segment of the distorted (6,0) SWGNT is shown with green and yellow balls.

TABLE 1: Symmetry, Average Binding Energy Per Atom ($\bar{E}_b$), Doping Energy (E_d), Total Magnetic Moment (M_t), Local Magnetic Moment of Dopants (M_M), Magnetic Moment of the Au_{24} Shell (M_{Au}), and Average Distances of Dopants from the Au_{24} Shell ($\bar{R}$)

cluster	symmetry	$\bar{E}_b$ (eV)	E_d (eV)	M_t (μ_B)	M_M (μ_B)	M_{Au} (μ_B)	$\bar{R}$(Å)
V@Au_{24}	D_{3h}	2.290	4.943	3	2.80	0.20	2.93
Cr@Au_{24}	C_{3h}	2.233	3.516	6	4.38	1.62	2.88
Mn@Au_{24}	D_{3h}	2.259	4.185	5	4.63	0.36	2.93
Fe@Au_{24}	C_{2v}	2.246	3.840	4	3.40	0.60	2.93
Co@Au_{24}	D_{3h}	2.236	3.596	3	2.09	0.91	2.93
Ni@Au_{24}	D_{3h}	2.249	3.921	2	1.16	0.84	2.91
Au_{24}	D_{3d}	2.194					2.81

tion via the Perdew−Wang exchange correlation functional.[28] The Accelrys DMOL^3 package was employed,[29] in which a double-numerical polarized basis set was chosen to describe the electronic wave functions. The scalar relativistic effects, such as the mass velocity and Darwin correction terms, were included in the semicore pseudopotential[30] calculations. All self-consistent field calculations were done with a convergence criterion of 10^{-6} au on the total energy and electron density. The cluster geometry was optimized by the Broyden−Fletcher−Goldfarb−Shanno algorithm[31] without symmetry constraints until the total energy was converged to 10^{-6} eV in the self-consistent loop and the force on each atom was less than 5 meV/Å. Vibrational frequency calculations and normal-mode analyses have been performed on the doped tubular clusters, and the infrared (IR) spectra have been calculated, confirming that they are true minima on the potential energy surface (PES).

The reliability of the current computational scheme was first checked by benchmark calculations on the Au_2 and Fe_2 dimers. The binding energy of 2.19 eV, bond length of 2.54 Å, and vibration frequency of 172.9 cm^{-1} were obtained for the gold dimer, which are all consistent with the experimental data of 2.28 ± 0.10 eV, 2.47 Å, and 191 cm^{-1}, respectively.[32] As for Fe_2, the calculated bond length of 2.00 Å is in excellent agreement with the experimental value of 2.02 Å.[33] Additionally, we have also calculated the magnetic moment of the $FeAu_{12}$ cluster with I_h symmetry and found that the local magnetic moment of Fe is 3.058 μ_B, which is comparable to the results of 3.064 μ_B with different basis sets reported in the previous ab initio studies.[14] The above results indicate that our method could well simulate the structures and properties of M@Au_{24} clusters.

III. Results and Discussion

Several tubular Au_{24} clusters, constructed by closing the SWGNTs with different helicities and diameters (from 4.5 to 8.3 Å) from appropriate ends, are chosen in our DFT calculations as the initial structures, based upon which two tubular structures with D_{3d} and D_{3h} symmetries, respectively, are finally determined as the ground-state and the first-lying tubular isomers after full geometry optimization. Among both of them, the former is composed of three six-member rings and two triangle caps on the two ends, which can be obtained by closing a segment of a distorted (6,0) SWGNT with two antisymmetric equilateral triangles. In the previous DFT studies, this tubular structure was identified as the ground state of the anionic Au_{24}^- by a joint electron diffraction measurement and local spin density functional molecular dynamics simulation method.[26] The latter was formed by sealing a segment of the (6,0) SWGNT but with two symmetric equilateral triangle caps and was separated from the former by 0.312 eV in energy. Our results on the pure Au_{24} cluster agree well with those of Zhao et al.[34]

Placing initially the transition-metal dopants M (M = V, Cr, Mn, Fe, Co, and Ni) at the center site of the tubular Au_{24} structures, we performed geometry optimizations without any geometric or symmetry constraint. The optimized stable structures of the M@Au_{24} cluster are displayed in Figure 1, from which it is clearly seen that the dopant atom does not significantly perturb the atomic structures of these two parent Au_{24} tubular frameworks but changes their energy's order, that is, making the higher-energy tubular Au_{24} cluster with D_{3h} symmetry become the ground one by doping a transition-metal atom. In addition, it is found that the ground-state M@Au_{24} (M = V, Mn, Co, and Ni) clusters still maintain the original D_{3h} structural symmetries, but Cr@Au_{24} distorts to C_{3h} symmetry, with the Cr atom deviating from the central site along the tube axis direction, and Fe@Au_{24} is subjected to a slight distortion, leading to a lower symmetry C_{2v}.[35]

In order to know the stabilities of the doped tubular M@Au_{24} clusters, we have compared their average binding energies (BEs) with that of the pure Au_{24} and given the obtained results in Table 1. The BE is calculated using $E_b = (E_M + 24E_{Au}) - E_{M@Au24}$, where E_M and E_{Au} are the energies of single M and Au atoms, respectively, while $E_{M@Au24}$ is the energy of the M@Au_{24}. It can be seen from Table 1 that all of the BEs/per atom for the M@Au_{24} clusters are larger than that of the ground-state pure Au_{24} cluster with D_{3d} symmetry. It should be noted that the ground-state pure Au_{25} cluster with a double-layered

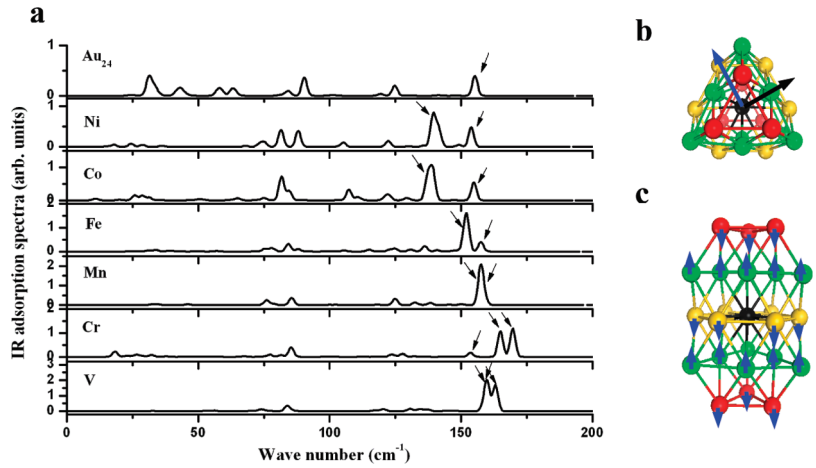

Figure 2. (a) The IR adsorption spectra of the M@Au_{24} and the Au_{24} host. The arrows, pointing to right and left, denote the characteristic peaks of dopants and the Au_{24} host, respectively. The schematics of the vibrational modes, corresponding to the IR characteristic peaks of the dopant and the Au_{24} tubular cage, are given for the Fe@Au_{24} cluster in (b) and (c), respectively, where the directions and amplitudes of the displacements are depicted by the corresponding vectors. The spectra are obtained by 1 cm^{-1} Gaussian broadening.

flat cage structure[34] is higher in total energy than all of the M@Au_{24} clusters by more than 1.2 eV. Therefore, the introduction of a transition-metal atom can enhance the stability of the tubular Au_{24} cluster. To further investigate the relative stabilities of the M@Au_{24} clusters, we also discuss their doping energy E_d, defined as $E_d = (E_M + E_{Au24}) - E_{MAu24}$, where E_{Au24} is the energy of the pure Au_{24} (D_{3h}) cluster. It can be seen from Table 1 that the V@Au_{24} cluster has the largest E_d of 4.943 eV, and the Mn@Au_{24} is the next one with its E_d of 4.146 eV, which indicates that both of them are more stable than other doped M@Au_{24} clusters.

For all of the tubular M@Au_{24} clusters, the frequency check was performed, and no imaginary frequencies were obtained, verifying that they are true minima on the potential energy surfaces. Since the geometrical structure of a cluster plays an important role in its physical and chemical properties, it is very useful to get its structural information, which may be done by a comparison of its infrared (IR) resonance-enhanced multiple photon dissociation spectroscopy with the DFT calculations, as made successfully for the neutral Au_n (n = 7, 19, and 20) clusters.[36] Therefore, we calculated the IR absorption spectra of the tubular M@Au_{24} clusters and pure Au_{24} (D_{3h}), which are shown in Figure 2. It can be seen clearly from Figure 2 that the IR spectra of the pure tubular Au_{24} are significantly changed by the dopants, which makes the IR spectra of the doped tubular M@Au_{24} depend sensitively on the different transition-metal atoms. The doping transition-metal atoms suppress the amplitudes of the low-energy vibrational modes in the IR spectra of pure tubular Au_{24} cluster and induce several new characteristic absorption peaks in its high-energy range (>100 cm^{-1}). For M@Au_{24} (M = Mn, Fe, Co, and Ni) clusters, these characteristic absorption peaks are found to lie at 158, 152, 139, and 140 cm^{-1}, respectively, which correspond to the doubly degenerate vibrational modes, involving only the dopant atoms' motions along the radial direction, known by the normal-mode analyses. For example, the characteristic absorption peak of the Fe@Au_{24} is found to be at 152 cm^{-1}, contributed to by the two doubly degenerate vibrations of the central Fe atom along the radial directions, whose normal-mode displacement vectors are shown in Figure 2b. However, for both V@Au_{24} and Cr@Au_{24} clusters, their characteristic dopant's absorption peaks split into two, lying at 160, 163 cm^{-1} and 165, 169 cm^{-1}, respectively, because their corresponding vibrational modes are not degenerate now. More interestingly, it is found that in all of the M@Au_{24} clusters from M = Ni to V, their Au_{24} host's IR characteristic peaks, indicated by the left arrows in Figure 2a, almost do not shift, but those of the dopant atoms, indicated by the right arrows in Figure 2a, make a blue shift, closing gradually to the Au_{24} host's IR characteristic peak, coinciding with it at M = Mn and then passing through it for M = Cr and V, as shown in Figure 2a. All of these characteristic IR spectra can be considered as the fingerprints of the endohedral M@Au_{24} clusters, which are helpful for identifying their structures in future experiments.

By doping a 3d transition-metal atom, its open d shell electrons are added to the composite gold cluster, introducing a local spin magnetic moment (LSMM). The calculated total magnetic moment M_t of the tubular M@Au_{24}, the LSMM of the impurity atoms M_M, and the magnetic moment M_{Au} of the gold host are given in Table 1. It is clearly seen that all of the tubular M@Au_{24} (M = V, Cr, Mn, Fe, Co, and Ni) are magnetic and that their M_t = 3, 6, 5, 4, 3, and 2 μ_B, respectively, are exactly equal to the atomic magnetic moment of the corresponding magnetic impurity atoms. Here, the tubular Au_{24} framework acts as a host, protecting the LSMM of the central dopant atoms. Mulliken atomic spin density analyses show that the spin densities mainly locate on the central dopants for all of these doped M@Au_{24} clusters and the magnetic metal atoms induce parallel spin polarization in the tubular Au_{24} cluster. It is found that all of the dopants in the tubular M@Au_{24}, except M = Cr with only one 4s electron, transfer their two 4s electrons to the parent Au_{24} framework, making the dopants possess their own atomic d-orbital valence configurations, which are similar to the situation of the golden cage M@Au_{16} clusters (M = Fe, Co, and Ni),[24] whose bonding states can be described as $M^{2+}@Au_{16}^{2-}$.

For a transition-metal impurity in a nonmagnetic host, the hybridization of the impurity d states with the host metal plays a crucial role in determining the local magnetic moments, which are sensitive to both the local structure and the electronic nature of the host. In the previous works, Wang et al.[14] investigated the LSMM of 3d impurities encapsulated in an icosahedral Au_{12} cage using a real-space first-principle cluster method, finding that the magnetic moments of M@Au_{12} clusters are 1, 2, 3, and 4 μ_B for M = Mn, Fe, Co, and Ni, respectively. The reason is explained by the strong hybridization between the dopants and the Au_{12} host of the M@Au_{12} clusters, in which the Mn and Fe atoms make the polarization of the Au_{12} cage antiparallel with their LSMMs while the Co and Ni atoms lead to the parallel

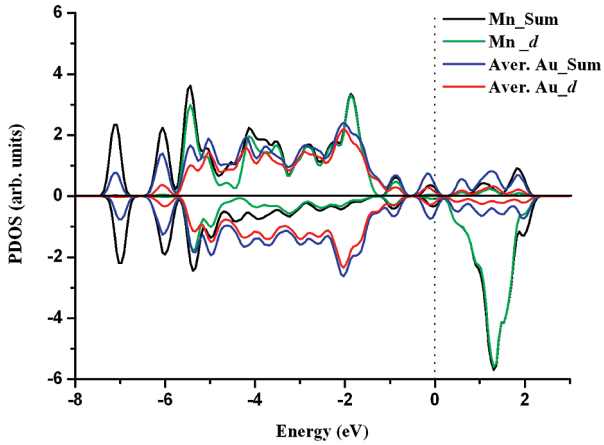

Figure 3. PDOSs of the Mn atom's d states and the Au_{24} host's d states for the tubular $Mn@Au_{24}$ cluster. For comparison, shown also are the average total DOSs of the Au_{24} host and the Mn atom. The spin-up and spin-down states are displayed in the up (positive) and down (negitive) panels, respectively. The dashed line indicates the location of the Fermi level. The DOSs are obtained by 0.1 eV Gaussian broadening.

polarization. On the other hand, Zhang et al.[37] found that the magnetic moments of the doped Au_6 clusters with the 3d transition-metal atoms (Mn, Fe, Co, and Ni) are 3, 2, 1, and 0 μ_B, respectively, which are most probably caused by the planar structure of MAu_6 clusters because the local magnetic moment of a transition-metal impurity atom strongly depends on its local environment. It is thus interesting to investigate different kinds of 3d transition-metal atom encapsulated in a gold cluster.

It is well-known that according to Hund's rules, an open-shell atom should be magnetic in its ground state. After they bind together, some discrete localized atomic orbitals could be delocalized or hybridized, making the system's magnetism be quenched in many bulk materials. For the bimetallic clusters made up of the transition-metal and noble metal atoms, the complex hybridization effects between the electrons of two different types of atoms would determine the magnetic properties of the mixed clusters. For our tubular $M@Au_{24}$ clusters, in order to explore the hybridization effect between the 3d electrons of transition-metal atoms and those of the Au_{24} host, we have calculated their spin-dependent partial density of states (PDOS). Taken as an example, the obtained results for the tubular $Mn@Au_{24}$ are given in Figure 3, from which we can see clearly that the hybridization mainly occurs between the Mn atom's 3d orbitals and the Au_{24} tubular host, lying in an energy range from about -5.5 to -1.5 eV. The spin-up and -down PDOSs of the Mn atom's d orbitals are quite different in the energy region, suggesting that the spin magnetic moments of the $Mn@Au_{24}$ cluster come mainly from the Mn atom's d states, which is consistent with the above Mulliken analyses on the atomic spin density.

On the other hand, we have also examined in detail the energy levels and corresponding molecular orbitals of the tubular $M@Au_{24}$ clusters, trying to find some characteristic orbtals which could show more clearly the localized spin orbitals at the dopant, and we have indeed found them. Here, taking the $Co@Au_{24}$ cluster as an example, we have shown two of them in Figure 4, lying at about 1.13 eV below its Fermi surface, which contributes about half of the total magnetic moment to the $Co@Au_{24}$ cluster. It can be clearly seen from Figure 4 that these two spin-up orbitals localize mainly at the central Co atom in comparison with the Au shell and display an obvious d-orbital character. Thus, it is obvious that the Au_{24} tubular framework

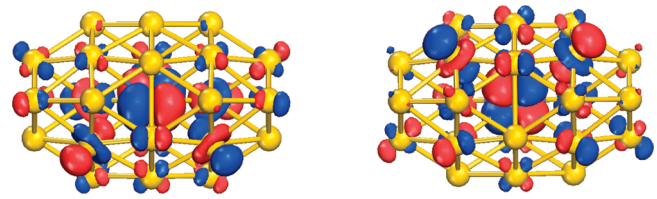

Figure 4. Two spin-up localized molecular orbitals of the $Co@Au_{24}$ cluster, whose energy levels are indicated below them, counted from its Fermi surface. (The isovalue is 0.02 au.)

acts as a host, protecting the spins of the central dopant atoms. Similar behavior is observed for all other $M@Au_{24}$ (M = V, Fe, Co, and Ni) clusters.

Finally, we should point out that the magnetic superatoms of $Cr@Au_{24}(SR)_{18}^-$, $Mn@Au_{24}(SR)_{18}$, and $Fe@Au_{24}(SR)_{18}^+$ have recently been predicted by magnetic doping of a gold cluster, are protected by the ligands, and are made by wet chemistry.[38,39] It has been found that these superatoms have 5, 5, and 3 μ_B magnetic moment, respectively, which are the same as those of our $Mn@Au_{24}$, $Cr@Au_{24}$, and $Fe@Au_{24}$ clusters, if charged.

IV. Conclusions

In summary, we have made our relativistic DFT studies on the stability and local spin magnetic moments of the tubular $M@Au_{24}$ clusters (M = V, Cr, Mn, Fe, Co, and Ni). It was found that (1) the encapsulations do not destroy the tubular frameworks of the gold host but change the energy's order of the pure Au_{24} isomers, showing a high possibility to form a novel binary alloy gold cluster with the tubular structures, (2) the ground states of most $M@Au_{24}$ still possess the D_{3h} structural symmetry of the host tubular Au_{24}, but both $Cr@Au_{24}$ and $Fe@Au_{24}$ have the lower symmetries of C_{3h} and C_{2v}, respectively, because the Cr and Fe dopants induce the slight structure distortions, (3) the IR spectra of the tubular Au_{24} cluster are significantly changed by the dopant atoms; for example, the characteristic absorption peaks appear in the IR spectra of all of the $M@Au_{24}$, which are induced by the dopant atoms' vibrational modes, and (4) protected by the tubular Au_{24} host, the 3d states of the dopant atoms are largely localized, which leads to the atom-like magnetism for all of the $M@Au_{24}$, exhibiting 3, 6, 5, 4, 3, and 2 μ_B for M = V, Cr, Mn, Fe, Co, and Ni, respectively.

Compared with previous studies on the transition-metal-doped gold clusters, we have found new tubular-encapsulated Au_{24} clusters with different transition-metal atoms, showing different local spin magnetic moments, which are very interesting in designing new nanomaterials with tunable magnetic properties.

Acknowledgment. This work was supported by the State Key program of China through Grants 2006CB921803 and 2009CB929504. W.F. also acknowledged support from the Research Fund for the Doctoral Program of Higher Education RFDP20070284055.

References and Notes

(1) Haruta, M. *Catal. Today* **1997**, *36*, 153. Haruta, M.; Kobayashi, T.; Sano, H.; Yamada, N. *Chem. Lett.* **1987**, *2*, 405.
(2) Daniel, M. C.; Astruc, D. *Chem. Rev.* **2004**, *104*, 293.
(3) (a) Pyykkö, P. *Angew. Chem., Int. Ed.* **2004**, *43*, 4412. (b) Pyykkö, P. *Nat. Nanotechnol.* **2007**, *2*, 273.
(4) (a) Häkkinen, H.; Moseler, M.; Landman, U. *Phys. Rev. Lett.* **2002**, *89*, 033401. (b) Häkkinen, H.; Yoon, B.; Landman, U.; Li, X.; Zhai, H. J.; Wang, L. S. *J. Phys. Chem. A* **2003**, *107*, 6168.

(5) Bulusu, S.; Li, X.; Wang, L. S.; Zeng, X. C. *Proc. Natl. Acad. Sci. U.S.A.* **2006**, *103*, 8326.
(6) Li, J.; Li, X.; Zhai, H. J.; Wang, L. S. *Science* **2003**, *299*, 864.
(7) Fa, W.; Luo, C. F.; Dong, J. M. *Phys. Rev. B* **2005**, *72*, 205428.
(8) Fa, W.; Dong, J. M. *J. Chem. Phys.* **2006**, *124*, 114310.
(9) (a) Johansson, M. P.; Sundholm, D.; Vaara, J. *Angew. Chem., Int. Ed.* **2004**, *43*, 2678. (b) Gu, X.; Ji, M.; Wei, S. H.; Gong, X. G. *Phys. Rev. B* **2004**, *70*, 205401.
(10) (a) Pyykkö, P.; Runeberg, N. *Angew. Chem.* **2002**, *114*, 2278. (b) Pyykkö, P.; Runeberg, N. *Angew. Chem., Int. Ed.* **2002**, *41*, 2174.
(11) Li, X.; Kiran, B.; Li, J.; Zhai, H. J.; Wang, L. S. *Angew. Chem., Int. Ed.* **2002**, *41*, 4786.
(12) Neukermans, S.; Janssens, E.; Tanaka, H.; Silverans, R. E.; Lievens, P. *Phys. Rev. Lett.* **2003**, *90*, 033401.
(13) Zhai, H. J.; Li, J.; Wang, L. S. *J. Chem. Phys.* **2004**, *121*, 8369.
(14) Wang, S. Y.; Yu, J. Z.; Mizuseki, H.; Sun, Q.; Wang, C. Y.; Kawazoe, Y. *Phys. Rev. B* **2004**, *70*, 165413.
(15) (a) Gao, Y.; Bulusu, S.; Zeng, X. C. *J. Am. Chem. Soc.* **2005**, *127*, 15680. (b) Gao, Y.; Bulusu, S.; Zeng, X. C. *ChemPhysChem* **2006**, *7*, 2275.
(16) Yuan, D. W.; Wang, Y.; Zeng, Z. *J. Chem. Phys.* **2005**, *122*, 114310.
(17) Li, X.; Kiran, B.; Cui, L. F.; Wang, L. S. *Phys. Rev. Lett.* **2005**, *95*, 253401.
(18) Majumder, C.; Kandalam, A. K.; Jena, P. *Phys. Rev. B* **2006**, *74*, 205437.
(19) Walter, M.; Häkkinen, H. *Phys. Chem. Chem. Phys.* **2006**, *8*, 5407.
(20) Wang, L. M.; Bulusu, S.; Zhai, H. J.; Zeng, X. C.; Wang, L. S. *Angew. Chem., Int. Ed.* **2007**, *46*, 2915.
(21) Wang, L. M.; Bulusu, S.; Huang, W.; Pal, R.; Wang, L. S.; Zeng, X. C. *J. Am. Chem. Soc.* **2007**, *129*, 15136.
(22) Sun, Q.; Wang, Q.; Chen, G.; Jena, P. *J. Chem. Phys.* **2007**, *127*, 214706.
(23) Sun, Q.; Wang, Q.; Jena, P.; Kawazoe, Y. *ACS Nano* **2008**, *2*, 341.
(24) Wang, L. M.; Bai, J.; Lechtken, A.; Huang, W.; Schooss, D.; Kappes, M. M.; Zeng, X. C.; Wang, L. S. *Phys. Rev. B* **2009**, *79*, 033413.
(25) Oshima, Y.; Onga, A.; Takayanagi, K. *Phys. Rev. Lett.* **2003**, *91*, 205503.
(26) Xing, X. P.; Yoon, B.; Landman, U.; Parks, J. H. *Phys. Rev. B* **2006**, *74*, 165423.
(27) Bulusu, S.; Li, L.; Wang, L. S.; Zeng, X. C. *J. Phys. Chem. C* **2007**, *111*, 190.
(28) (a) Perdew, J. P. In *Electronic Structure of Solids '91*; Ziesche, P., Eschrig, H., Eds.; Akademie: Berlin, Germany, 1991. (b) Perdew, J. P.; Chevary, J. A.; Vosko, S. H.; Jackson, K. A.; Pederson, M. R.; Singh, D. J.; Fiolhais, C. *Phys. Rev. B* **1992**, *46*, 6671.
(29) DMOL^3 is a DFT-based package with the atomic basis distributed by Accelrys as a part of Materials Studio. See also: Delley, B. *J. Chem. Phys.* **1990**, *92*, 508.
(30) Delley, B. *Phys. Rev. B* **2002**, *66*, 155125.
(31) Fletcher, R. *Practical Methods of Optimization*; Wiley: New York, 1980; Vol. 1.
(32) (a) *CRC Handbook of Chemistry and Physics*, 55th ed.; Weast, R. C., Ed.; CRC: Cleveland, OH, 1974. (b) *American Institute of Physics Handbook*; McGraw-Hill: New York, 1972.
(33) Morse, M. D. *Chem. Rev.* **1986**, *86*, 1049.
(34) Tian, D. X.; Zhao, J. J. *J. Phys. Chem. A* **2008**, *112*, 3141.
(35) The coordinates for the optimized structures of M@Au_{24} can be obtained upon request to the authors (yapaping@gmail.com).
(36) Gruene, P.; Rayner, D. M.; Redlich, B.; van der Meer, A. F. G.; Lyon, J. T.; Meijer, G.; Fielicke, A. *Science* **2008**, *321*, 674.
(37) Zhang, M.; He, L. M.; Zhao, L. X.; Feng, X. J.; Luo, Y. H. *J. Phys. Chem. C* **2009**, *113*, 6491.
(38) Reveles, J. U.; Clayborne1, P. A.; Reber, A. C.; Khanna1, S. N.; Pradhan, K.; Sen, P.; Pederson, M. R. *Nat. Chem.* **2009**, *1*, 310.
(39) Jiang, D.; Whetten, R. L. *Phys. Rev. B* **2009**, *80*, 115402.

JP908511M